A Technique for Mapping the Distribution of Diffuse Solar Radiation over the Sky Hemisphere[1]

L. J. BRUCE MCARTHUR

Department of Geography, McMaster University, Hamilton, Ontario, Canada L8S 1K4

JOHN E. HAY

Department of Geography, The University of British Columbia, Vancouver, British Columbia, Canada V6T 1W5

(Manuscript received 30 May 1980, in final form 1 December 1980)

ABSTRACT

A technique to map the distribution of diffuse solar radiation over the sky hemisphere is described. The method is based on an analysis of all-sky, visible photographs and concurrent actinometric measurements of diffuse solar radiance. The photographs were digitized and the resulting relative density values correlated with directly measured radiances. The resulting relationship was then used to determine the radiance for each density value, enabling a map of diffuse solar radiation for the celestial dome to be constructed.

The validity and utility of the approach are assessed by several tests. In the first test, the estimated radiances were integrated over the hemisphere and compared with measured diffuse irradiances for a horizontal surface. These were found to be within ±10% for the variety of sky conditions examined. A second test, under clear sky conditions, was performed to estimate the shortwave irradiance on several south-facing inclined surfaces. The results were found to be within ±5% of the measured irradiances. In a third test, comparisons with the normalized radiance distributions of Steven (1977) indicated good qualitative agreement.

Finally, problems and deficiencies in the technique are reviewed and possible means of surmounting them are discussed.

1. Introduction

With the increasing interest in solar radiation as a source of energy, there is growing demand for information on the amount of short-wave radiation incident on an inclined surface. The determination of the diffuse shortwave irradiance for such inclined surfaces requires a knowledge of the spatial distribution of diffuse radiation over the sky hemisphere (Norris, 1966). This distribution can be determined through numerical modeling using model atmospheres (e.g., Dave, 1977); by empirically determining radiance values for given positions in the celestial dome (e.g., Morris and Lawrence, 1971; Hooper and Brunger, 1979); or through direct or indirect measurement techniques. Steven (1977) used a Linke Feussner actinometer to measure the radiance distribution of clear skies on 67 occasions. With the 34 observations for each of the 67 data sets, Steven was able to produce standard normalized radiance distributions for various zenith angles. However, because of the 40 min required to make such observations, the measurement technique he used is limited to the cloudless case.

The technique developed in the present study is an attempt to overcome the problem of instrument response time by supplementing the actinometric measurements with all-sky photographs. Section 2 describes the methods used to convert a dense sampling of density values taken from 35 mm all-sky photographs into equivalent radiance values. The validity of this approach is assessed in Section 3 by comparing the integrated radiances obtained via the photographs with measured irradiances for both horizontal and south-facing surfaces. The derived clear-sky radiance distributions are also compared with the measured distributions of Steven (1977). In Section 4 individual examples of radiance distributions for clear, partly cloudy and overcast skies are used to demonstrate both the complexities of the distributions and the major influence of cloud.

2. Methods

a. Field observations

All the data analyzed in this study were observed at the University of British Columbia Climatological

[1] The research reported in this paper derives from the M.Sc. thesis of the senior author.

0021-8952/81/040421-09$06.25

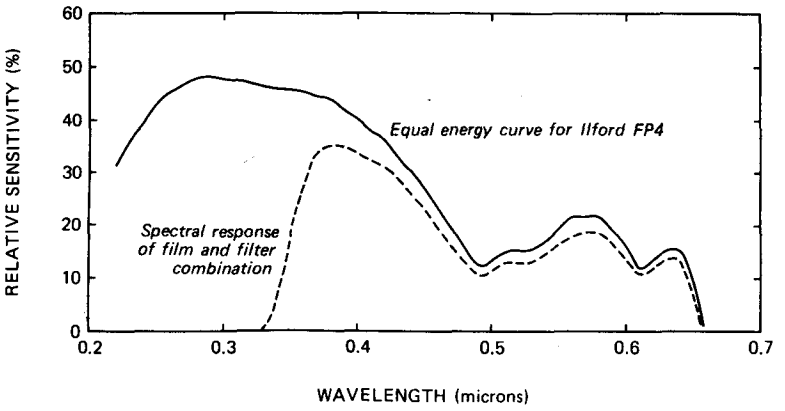

FIG. 1. Film and filter spectral response curves.

Station, Vancouver, Canada (49°15'N, 123°15'W). Observations were restricted to within 3 h of solar noon in February 1978 and during that time a wide range of cloud conditions (cloudless, partly cloudy, overcast) were sampled by 12 data sets. A data set consisted of 21 actinometric measurements and three pairs of all-sky photographs. The radiance measurements were made using a Linke Feussner actinometer (10° field of view) and a regular sampling grid over the sky hemisphere. The sampling pattern was designed to minimize actinometer movement between observations and to limit biasing errors when several sets of observations are combined (Steven, 1977). The restriction to 21 observation points was an arbitrary compromise between the need for high spatial resolution, the response time of the sensor and the temporal variability of the radiance distribution. An individual data set required ~14 min to acquire. The photographs were exposed at 2.0, 6.67 and 11.33 min from the beginning of each sequence of actinometric measurements.

The all-sky photographs were obtained using a Canon F-1 35 mm SLR camera with a Canon Fisheye 7.5 mm $f/5.6$ S.S.C. equidistant lens and a built in ultraviolet cutoff filter L-1B. This filter eliminates all radiation at wavelengths < 0.32 μm and provides a nearly flat transmittance curve for wavelengths between 0.4 and 2.4 μm. The photographic film was Ilford FP4, ASA 125. Relative to other small format films the sensitivity is relatively independent of wavelength over a wide wavelength range. This feature and the resulting spectral sensitivity of the filter-film combination are shown in Fig. 1.

The exposed film was processed by a professional processing company with one of the photograph pairs being redundant except when flaws occurred in the negative. No intra-film comparisons were carried out since a radiance calibration for each negative was required. A common calibration for all exposures would have placed severe limitations on camera exposure settings and the developing of the film.

Reduction of the photographic negatives into a digital form was accomplished using a Joyce Loebel Automatic Recording Densitometer (Fraser, 1978),[2] with an Autodensidater attachment. A 0-3D (neutral density units) optical wedge was used as calibration to maintain comparability between negatives. This density range was linearly divided into 1000 units to produce the relative density scale used in calibrating the photographic exposures with the actinometric measurements.

Mean density measurements from a 5625 μm^2 area were obtained every 400 μm in both X and Y coordinates. This provides 2629 density values over the exposed portion of the negative. The adequacy of this sample size is discussed by McArthur and Hay (1980). The consistency in maintaining the alignment and exact grid location between negatives on the microdensitometer is estimated to be within ± 25 μm in the X coordinate and ± 10 μm in the Y coordinate. An error of ± 25 μm represents less than 0.2° in both the zenith and the azimuth at a solar zenith angle of 60°. The internal consistency of the instrument to repeat a scan is ± 5 μm.

To most efficiently provide data from all sectors of the sky the diffuse radiance was measured using a regular sampling grid. Auxiliary measurements of direct beam, diffuse, reflected and total incoming radiation for 0, 30, 60 and 90° south-facing surfaces also were obtained during the observation period (Hay, 1979).[3]

The average probable error in the acquisition of the data, including the auxiliary measurements

[2] Fraser, I., 1978: Evaluating images quantitatively. *Canadian Research*, January/February, 27–28, 39.

[3] Hay, J. E., 1979: *A study of shortwave radiation on non-horizontal surfaces*. Canadian Climate Centre, Rep. No. 79-12, Atmospheric Environment Service, Downsview, 141 pp.

used in verification of the technique, is 7.5%. This error is based on both measurements taken during stable radiation conditions and the estimated probable error of the instruments involved in the study. This error has the same order of magnitude as that associated with the usual method of obtaining diffuse solar irradiance (4.2–4.6%) (Latimer, 1972).[4] However, this latter method does not provide any knowledge of the angular distribution of the diffuse radiation.

b. Photographic calibration

Since the photographic process samples < 10% of the solar spectrum, the technique described here relies on the amount of energy in this restricted portion of the solar spectrum being correlated with the amount of energy in the entire spectrum, not only over time but also for the various points over the sky hemisphere. Kondratyev *et al.* (1955) have shown good agreement between the distributions of radiance and luminance over the sky hemisphere, with the clear-sky case also being confirmed by the work of Dorno (1919) and Steven (1977). On the basis of this agreement it should be possible to develop an empirical relationship between the densities determined from the exposed negative and the corresponding radiances. Due to the possibility of the calibration being dependent on the spectral distribution of the radiation, it was important that the photographic data be calibrated *in situ* rather than through the use of laboratory-based techniques. The following paragraphs describe the approach used in the present study.

For each position of an actinometric measurement of solid angle 0.025 sr an average density for an area equivalent to 0.031 sr is determined using thirteen of the digitized photographic data points. These values and the corresponding actinometric values provide the data set on which the calibration curve for the entire photograph is based. Two curve-fitting procedures were tested. The first method correlated the complete actinometric data set with the density data for each of the three photographs exposed during a single actinometric measuring sequence. The second approach attempted to relate to the actinometric data, the density values only from those photographs which were exposed closest to the time of the radiance measurements. In this way the density values from a given photograph were paired with approximately one-third of the actinometric data. The three data sets were subsequently combined to yield a common calibration curve. The confidence levels for the calibration curves obtained using the latter approach were found to be highly variable. In stable radiation conditions the first method out-performed the "combination" technique while in overcast conditions the combination technique was superior. However, this advantage did not extend to the more complex partly cloudy conditions. Therefore, the actinometric measurements and density values obtained from a single photograph were used to derive the calibration curve.

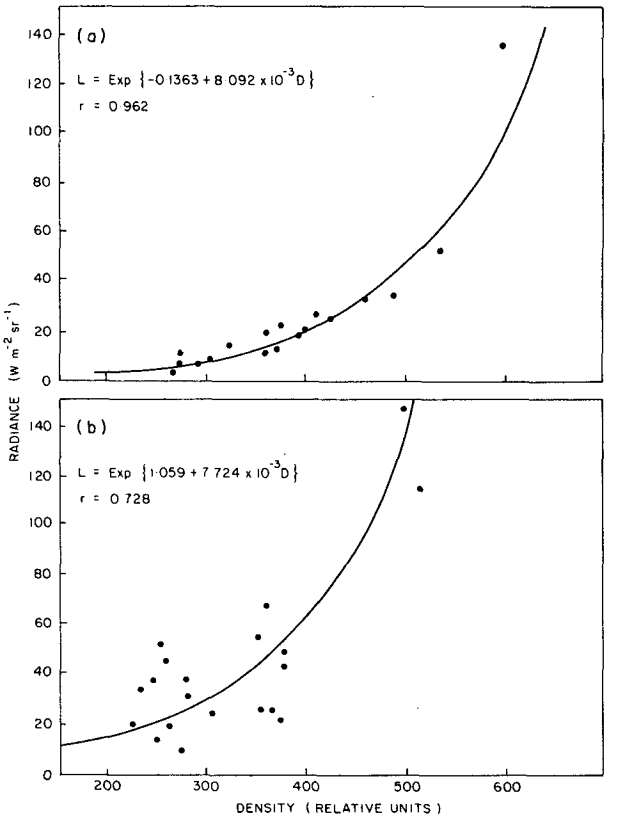

FIG. 2. Calibration curves for data gathered under (a) clear sky and (b) cloudy conditions.

It was hoped that a common form of calibration equation could be found to fit all radiance distributions. However, this was not the case. Of the 12 sets of observations investigated, seven were found to yield exponential curves, while the remainder required a variety of polynomial fits to hand-drawn curves. Of the seven exponential curves, three were clear-sky cases, while 4 were observations taken during partly cloudy conditions. Fig. 2 illustrates the results of fitting calibration curves to data gathered under clear sky and partly cloudy conditions. In the most complex and variable conditions it was found that no readily available curve-fitting procedure accurately defined a calibration curve for the data. In such cases a smooth hand-drawn curve was used as the basis for the required calibration equation. This approach was especially necessary in

[4] Latimer, J. R., 1972: *Radiation measurement*. IFYGL Tech. Manual Ser., No. 2, Queen's Printer, Ottawa, 53 pp.

the case of overcast conditions where the actinometric observations occurred within a small range of density values.

The calibration equations can be applied to individual density values yielding radiance distributions which are subsequently mapped using standard computer plotting routines.

3. Verification

The first test of the resulting radiance distributions was based on the method outlined by Steven (1977). This test assumes a unique relationship between the angular distribution of radiance and the observed diffuse irradiance. Thus, if the calculated irradiance was found to approximate the observed, the angular distribution was assumed correct. McArthur and Hay (1980) have investigated the validity of this assumption.

The numerical integration equation used to derive the irradiance for a horizontal surface from the radiance distribution follows the integral outlined in Paltridge and Platt (1977):

$$D_c^{\downarrow} = \sum_{i=1}^{n} L_i \delta\omega \cos z_i, \qquad (1)$$

where

$D_c^{\downarrow}$ calculated diffuse irradiance on a horizontal surface (W m^{-2})
L_i radiance from the point i (W m^{-2} sr^{-1})
$\delta\omega$ solid angle represented by each density (sr)
z_i zenith angle for the point i (rad)
n number of density values (2629).

Table 1 provides a comparison between measured irradiances and those derived using this approach. In the two cases that have a difference $> 10\%$ measurements were taken during fluctuating radiation conditions. Further, for the 24 February case, it was found that a large percentage of the actinometric observations occurred within a small range of density values. These differences in the accuracy of the diffuse irradiance estimates are a result of variations in the goodness of fit of the curve to the calibration data. Nevertheless, the relative error is generally very small especially in light of the probable error of 7.5%.

In a second test of the photographic technique the diffuse irradiance for three south-facing surfaces is estimated. This is a more rigorous evaluation of the quality of the angular distribution and thus provides a better test than did the horizontal surface in evaluating the ability of the photographic technique to map sky radiance. The importance of the radiance from a given point is either enhanced or lessened as the slope of the receiving surface changes. Only if the actual angular distribution is isotropic or correctly determined will the relative error in the technique be maintained over a number of surfaces of varying orientation.

Since the measurements of incoming solar radiation on the sloping surfaces and the direct beam measurements were obtained as 5 min integrated values, only clear-sky conditions could be utilized. The major difficulty in verifications using inclined surface data is the problem of radiation reflected onto the sloping surfaces. To determine the reflection by the horizontal surface the albedo of that surface was measured and the reflection assumed isotropic (Paltridge and Platt, 1976). The irradiance was then simply transformed to the appropriate slope angle using the method of Kondratyev (1969).

For those surfaces (commonly trees) extending above the theoretical horizon to form a local horizon, it was assumed that the albedo was 0.14 and that the reflection was also isotropic. Thus, from any given grid point found between the local and theoretical horizons, the amount of energy incident on the sloping surface is dependent on the cosine of

TABLE 1. Comparison of measured and computed diffuse irradiances. The computed values are derived from photographically determined radiances and Eq. (1).

Local apparent time	Date	Sky condition	Measured $D^{\downarrow}$ (W m^{-2})	Computed $D^{\downarrow}$ (W m^{-2})	Difference (W m^{-2})	Difference (%)
1240	10 Feb	clear	65.730	68.467	2.737	4.16
1340	10 Feb	clear	56.480	59.896	3.416	6.05
1120	14 Feb	10/10St	88.566	76.199	12.367	13.96
1230	14 Feb	10/10St	63.346	62.090	1.256	1.98
1247	15 Feb	8/10Ac	291.657	265.807	25.850	8.86
1317	15 Feb	4/10Ac 3/10Ci	162.552	167.802	5.25	3.23
1322	15 Feb	4/10Ac 3/10Ci	141.118	129.481	11.637	8.25
1347	15 Feb	3/10Ac 1/10Ci	91.561	90.586	0.975	1.06
1007	24 Feb	1/10Ac 5/10As 3/10Ci	199.108	165.000	34.108	17.13
1326	26 Feb	clear	52.550	55.059	2.509	4.77
1347	26 Feb	clear	51.590	50.715	0.875	1.70
1411	26 Feb	clear	49.680	49.088	0.592	1.19

the angle of incidence. The total amount of energy from this area [in the present study the horizon obstructions had a view factor (Steyn, 1980) of 0.02] is approximated by the summation of the product of the reflected energy at each grid point and the cosine of the angle of incidence of that energy on the inclined surface.

The diffuse component of the inclined surface irradiance is then found by summing the radiation obtained by numerically integrating the radiance over the appropriate portion of the celestial dome, the horizontal surface reflection onto the slope and the summation of the reflected component from each of the grid points between the theoretical and local horizons.

Table 2 provides the results of using this technique to determine the diffuse component of the shortwave irradiance for five clear-sky cases. The table includes differences between the measured 5 min mean irradiance and irradiances calculated using the photograph exposed during the integration period and the total shortwave irradiances calculated using an anisotropic diffuse radiation model (Hay and Davies, 1980). Even with the large possible error involved in the calculation of radiation reflected onto the sloping surfaces, the photographic technique consistently outperformed the anisotropic model on a 5 min average. The small errors in the photographically based irradiances would further suggest that that technique adequately reproduces the angular distribution of the diffuse radiance of the sky.

A third verification approach is also only applicable to clear-sky conditions. Based on the equivalent flux density relationship of Unsworth and Monteith (1975), the clear-sky radiance distributions were normalized to be directly comparable with those of Steven (1977). Fig. 3 presents the five clear-sky radiance normalized distributions, comparable to the distributions presented by Steven (1977) (Fig. 4). The isolines are set 0.5 sr^{-1} apart, similar to those of Steven. One immediately notices that despite the greater complexity of the present distributions the general agreement is good. Moreover, considering the two diagrams of Steven (for solar zenith angles of 35 and 55) and the general pattern of the normalized distribution for a zenith angle of 65° (Fig. 3e) as a time sequence, a number of the apparent differences can be explained. As the solar zenith angle increases, it appears that the general form of the 1.0 sr^{-1} isopleth changes from being generally circumsolar to encompassing the region of the sky hemisphere of least radiant intensity. This indicates that as the solar path in-

TABLE 2. Comparison of measured and calculated values of shortwave irradiance for a horizontal surface and three south-facing slopes.

Local Apparent Time of photograph	Slope (deg)	Measured* irradiance (W m^{-2})	Photographic technique		Anisotropic model (Hay and Davies, 1980)	
			Calculated (W m^{-2})	Difference (%)	Calculated (W m^{-2})	Difference (%)
1240	0†	460.41	440.76	−4.26**	440.76	−4.26**
	30	849.68	802.54	−5.54	799.24	−5.94
	60	1018.26	973.65	−4.38	963.79	−5.35
	90	944.37	902.79	−4.40	890.28	−5.73
1340	0	383.29	381.88	−0.37	381.88	−0.37
	30	734.90	710.75	−3.29	710.24	−3.35
	60	866.42	871.56	0.59	865.99	−0.05
	90	852.60	815.66	−4.33	807.39	−5.30
1326	0	525.12	507.33	−3.38	507.33	−3.38
	30	874.03	847.07	−3.08	843.62	−3.47
	60	995.04	986.35	−0.87	974.65	−2.05
	90	891.61	888.72	−0.32	872.38	−2.16
1347	0	494.78	475.74	−3.85	475.74	−3.85
	30	830.76	809.90	−2.51	802.87	−3.36
	60	959.29	941.99	−1.80	924.56	−3.62
	90	850.52	847.03	−0.41	824.81	−3.02
1411	0	449.47	433.97	−3.45	433.97	−3.45
	30	763.25	715.85	−2.28	740.56	−2.97
	60	870.94	868.68	−0.24	845.98	−2.87
	90	792.69	800.42	0.98	781.48	−1.41

* All measured values are 5 min mean fluxes centered on the time of the photograph.
** All negative values indicate an underestimation.
† 0° is defined as a horizontal surface.

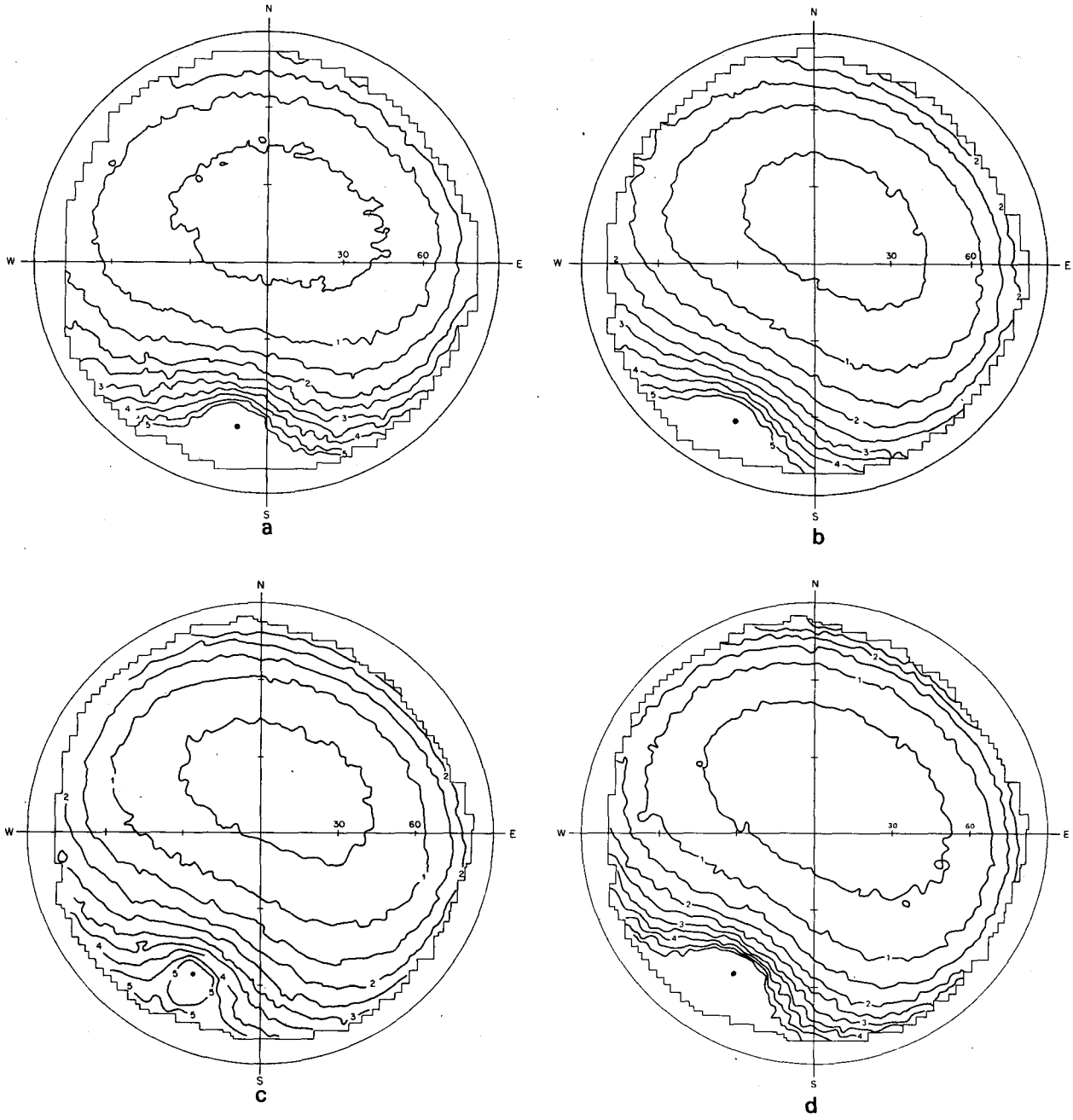

FIG. 3. Clear sky normalized sky radiance distribution (sr^{-1}) as produced from the photographic negative for: (a) 1240 LAT 10 February 1978 (solar zenith angle 64.5°); (b) 1340 LAT 10 February 1978 (solar zenith angle 67.6°); (c) 1326 LAT 26 February 1978 (solar zenith angle 61.0°); (d) 1347 LAT 26 February 1978 (solar zenith angle 62.8°); (e) 1411 LAT 26 February 1978 (solar zenith angle 65.0°).

creases, the limb brightening becomes relatively more important due to the increase in scattering mass. Correspondingly, in these normalized distributions the magnitude of the isoline closest to the solar disc increases with the increase in the solar zenith angle. This is also a result of the increasing scattering mass and the strong forward peak of the Mie scatter about the solar disc.

As the solar zenith angle approaches 90°, the pattern of clear sky radiance becomes more complex. This is illustrated by Fig. 4b and Figs. 3c to 3e where the solar zenith angles are 55, 61, 62.8 and 65°, respectively. For a solar zenith angle of 55° the circumsolar region is well defined by continuous isolines. However, by a solar zenith angle of 61°, only the 5 sr^{-1} circumsolar isoline is continuous.

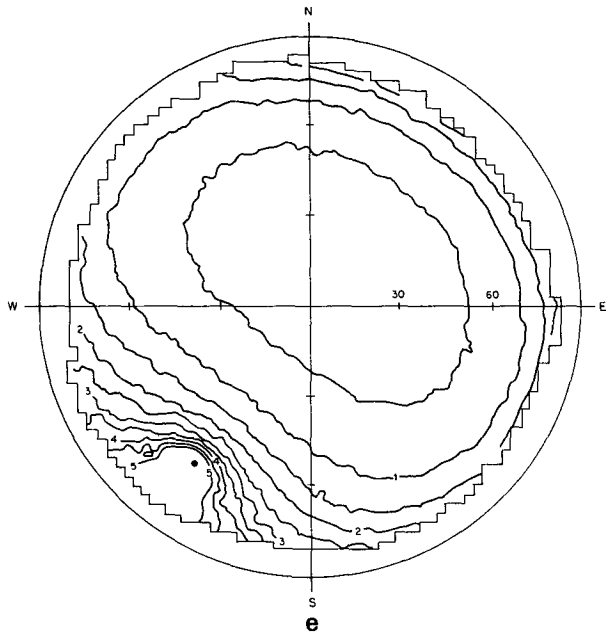

FIG. 3. (*Continued*)

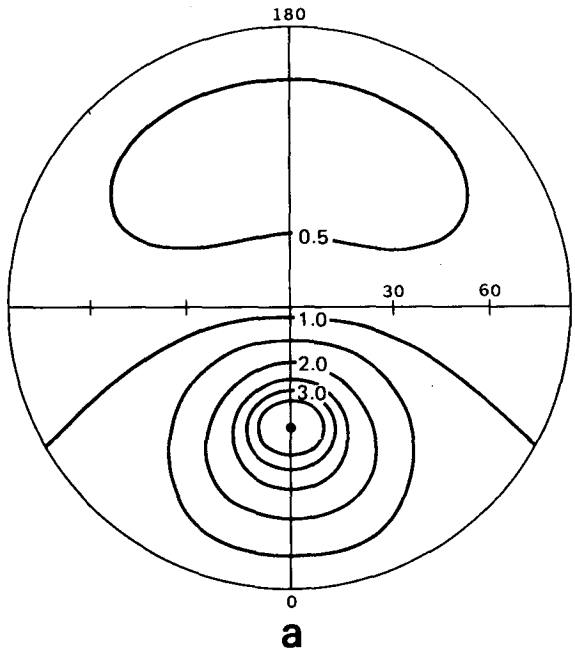

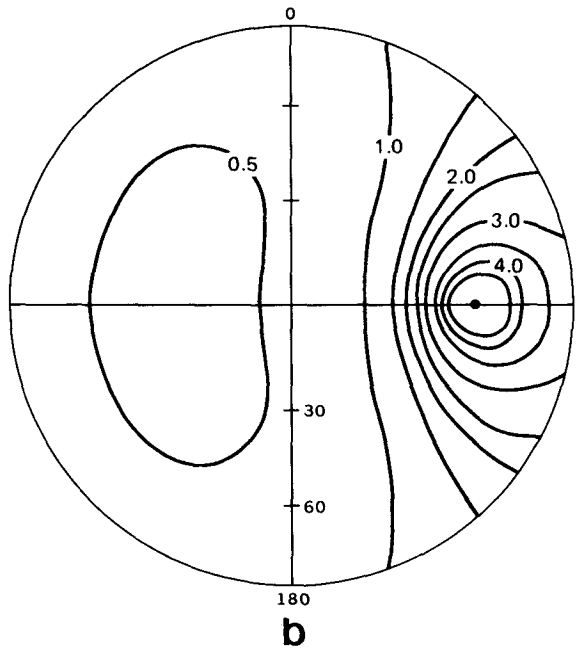

FIG. 4. Standard distribution of normalized sky radiance of Steven (1977). Isopleths (sr^{-1}) are equivalent on each diagram. (a) Solar zenith angle 35°, (b) solar zenith angle 55°.

In the normalized maps for solar zenith angles > 61° (Figs. 3d and 3e), no continuous circumsolar isolines are observed. The 4.5 sr^{-1} isoline in Fig. 4b is seen to be continuous, while with a 6° increase in solar zenith angle (Fig. 3c), it is discontinuous and influenced by limb brightening. By the time a zenith angle of 62.8° is reached (Fig. 3d), the 5 sr^{-1} isoline is also found to be affected by scattering near the horizon. With a solar zenith angle of 65° (Fig. 3e), the increased scattering of radiation due to the large optical air mass commences to dominate the scattering within the circumsolar region indicating its eventual total breakdown (Morris and Lawrence, 1971). As the solar zenith angle increases, the diffuse radiance emanating from the region about the horizon is an increasingly significant percentage of the diffuse irradiance.

Thus, qualitatively, the two sets of normalized radiance distributions appear to be compatible. This gives further evidence that the photographic technique is appropriate for the strongly anisotropic clear sky case. Further, since the processes are identical for both cloudless and the spatially more complex cloudy sky cases, the technique should be capable of mapping the overcast and partly cloudy radiance distributions. Results for these cloud conditions will be presented in the following series of case studies.

4. Case studies

Figs. 5–7 provide examples of the radiance maps produced for clear, partly cloudy and overcast skies as seen on an equidistant projection. The photographic technique, with its rapid response time and high spatial resolution is eminently suited to investigating the complex radiance distributions occurring with partly cloudy skies. The isolines range between 5 and 130 W m^{-2} sr^{-1} with intermediate values of 10, 20, 30, 40, 60, 80 and 105 W m^{-2} sr^{-1}. These values provide the best coverage

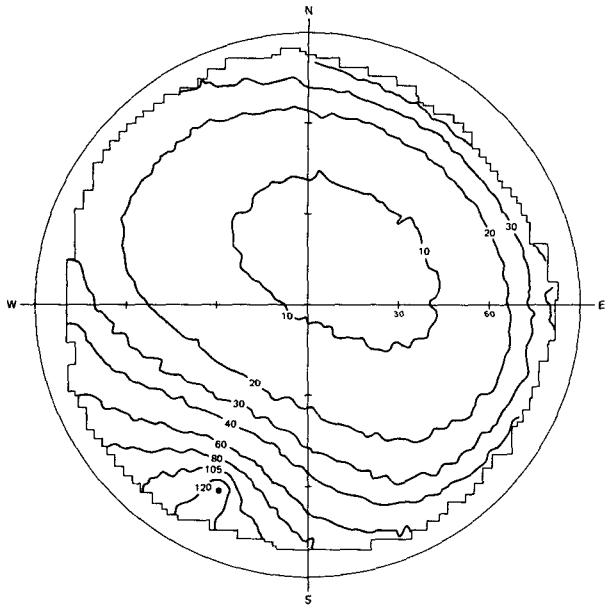

FIG. 5. Diffuse radiance (W m^{-2} sr^{-1}) distribution for a clear sky as produced from the photographic negative for 1340 LAT 10 February 1978; solar zenith angle 67.6°.

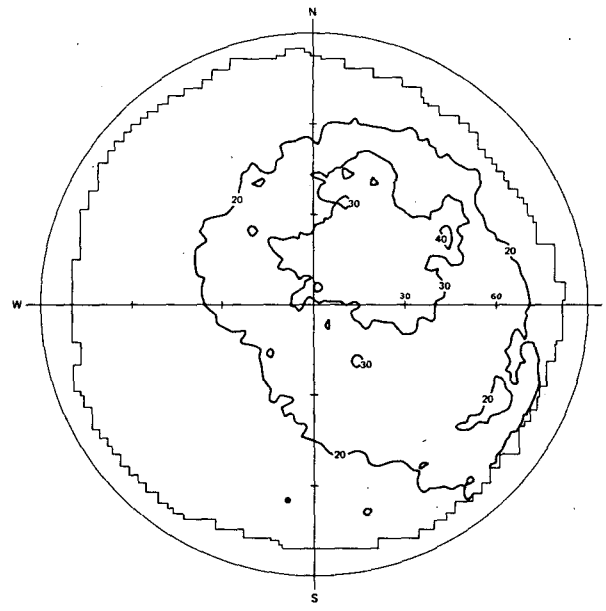

FIG. 7. As in Fig. 5 except for an overcast sky at 1230 LAT 14 February 1978, solar zenith angle 63.0°.

of the celestial dome for both clear and cloudy conditions. The irregular intervals provide the necessary means to encompass with a minimum of isolines, both the very low radiance values 90° from the sun and the high values around the solar disc.

Fig. 5 is the clear sky radiance pattern for 1340 Local Apparent Time (LAT) 10 February. The least intense sky radiance is found ~90° from the solar disc with the intensity increasing from there out to the horizon. This increase follows a nearly elliptical pattern until it is influenced by the circumsolar region (Morris and Lawrence, 1971, Hooper and Brunger 1979). At this point, the radiance isolines (isorads) are influenced more by the solar disc and begin to follow concentric patterns around the sun.

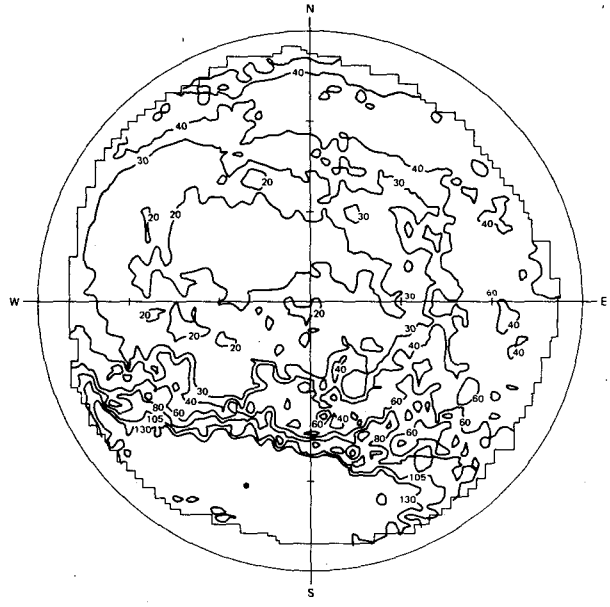

FIG. 6. As in Fig. 5 except for a partly cloudy sky at 1317 LAT 15 February 1978, solar zenith angle 64.5°.

In the partly cloudy condition of 1317 LAT 15 February (Fig. 6), the lowest intensity occurs in the same region. However, the magnitude of the intensity has increased due to the greater scattering effect of the water droplets. The intensity increases both toward the horizon and the solar disc, but not in the same consistent pattern as the clear-sky case. In addition, the area around the solar disc is not the only area of the hemisphere where the radiance is greater than 130 W m^{-2} sr^{-1}. The cause is the large radiance from the highly reflective cloud elements located near the sun and the resulting pattern illustrates the complexity that cloud introduces into the distribution of diffuse radiance.

Fig. 7 illustrates that in heavy overcast the gradient has almost completely diminished and the solar position is not even evident. Kondratyev (1969) states, "that for a dense non-transparent cloudiness, the azimuthal dependence of diffuse radiation intensity is not marked enough and a somewhat monotonous increase of the intensity from the horizon zenithward is observed." Although the commonly invoked isotropic assumption is not met in any of the above cases, Fig. 7 indicates that for dense cloud the approximation is reasonably valid over the central portion of the sky. In all other conditions, however, the radiance is strongly anisotropic, suggesting that models which invoke this assumption

(e.g., ASHRAE, 1975)[5] are neglecting an important factor when calculating the irradiance for a given surface.

5. Conclusions

The study presents a technique to determine the angular distribution of diffuse radiation in the sky hemisphere. The advantages of this method over previous instrumental studies are

1) The present technique provides an instantaneous mapping of the celestial dome. Even the most complex diffuse radiance conditions can now be mapped.

2) The sample size employed is two orders of magnitude larger than that used in previous studies. Therefore, the maps produced using this method provide greater detail and are significantly more precise than those previously published.

3) The diffuse radiance data base is in digital form and is evenly and densely distributed over the sky hemisphere allowing it to be used with little manipulation to determine the diffuse irradiance on inclined surfaces.

However, the technique has not yet been perfected, nor are the results comprehensive enough for generalizations to be made. The approach described here is restricted by the need to make observations of the diffuse radiance in order to calibrate the photographic data. The accuracy of these calibrations is reduced by the same limitations of the actinometer (response time, field of view) that the photographic technique is attempting to avoid. The quality of the calibrations could be improved if a faster response instrument with a narrower field of view was utilized. Ideally, if there was a universal calibration relating film density and radiance the latter measurements would not be required. However, such a consistent relationship between these two variables is improbable due to the wavelength dependence of the atmospheric absorption and scattering processes, the inconsistencies in the manufacture and processing of the photographic film which has a limited spectral response and the use of various exposure settings when the film is exposed. Some of these difficulties could be alleviated with the use of specialized photographic plates available for the larger format cameras. Moreover, for the conditions examined in this paper, workable relations between film density and radiance were developed, though further testing would be desirable in order to assess the sensitivity of the calibration relationships to changes in aerosol concentration and to the conditions prevailing with small solar zenith angles.

With the established ability to determine radiance distributions for a wide variety of sky conditions it is now appropriate to consider the use of a large number of such observations to confirm the claim of Steven (1977) that a standardized clear-sky radiance distribution does exist and attempt to specify some general features for the more complex distributions which occur under partly cloudy conditions. Such information would be invaluable to researchers who are using numerical models to evaluate the distributions of the diffuse radiance over the sky hemisphere and to the modellers of shortwave irradiance for inclined surfaces.

Acknowledgments. The financial support for this study was provided by the Canadian Natural Sciences and Engineering Research Council and the Canadian Atmospheric Environment Service. Their assistance is greatly appreciated. The measurement program was conducted at the University of British Columbia Climate Field Station which is under the supervision of Mr. D. Pearce. Mr. P. Jance drafted the diagrams.

[5] ASHRAE, 1975: American Society of Heating, Refrigerating and Air Conditioning Engineers. *Procedure for Determining Heating and Cooling Loads for Computerized Energy Calculations. Algorithms for Building Heat Transfer Subroutines*, 169 pp.

REFERENCES

Dave, J. V., 1977: Validity of the isotropic distribution approximation in solar energy estimations. *Solar Energy*, **19**, 331–333.

Dorno, D., 1919: Himmelshelligkeit, Himmelspolarisation und Sonnenintensität 1911–1918. *Veröffent. Preuss. Meteor. Inst.*, **6**, No. 303, 306 pp.

Hay, J. E., and J. A. Davies, 1980: Calculation of solar radiation incident on an inclined surface. *Proc. First Canadian Solar Radiation Data Workshop*, J. E. Hay and T. K. Won, Eds., Canadian Atmospheric Environment Services, Downsview, Ontario, 166 pp.

Hooper, F. C., and A. P. Brunger, 1979: A model for the angular distribution of sky radiance. *J. Solar Energy Eng.*, **102**, 196–202.

Kondratyev, K. Ya., 1969: *Radiation in the Atmosphere*. Academic Press, 912 pp.

——, L. A. Kudriavtzeva and M. P. Manolova, 1955: Distribution of the energetical and light intensity of diffuse atmospheric radiation over the celestial sphere. *Bull. Leningrad Univ.*, 119–129.

McArthur, L. J. B., and J. E. Hay, 1980: An assessment of the techniques for determining the distribution of diffuse solar radiance for the sky hemisphere. *Solar Energy*, **25**, 573–574.

Morris, C. W., and J. H. Lawrence, 1971: The anisotropy of clear sky diffuse solar radiation. *ASHRAE Trans. 1971*, Part II, **77**, 136–141.

Norris, D. J., 1966: Solar radiation on inclined surfaces. *Solar Energy*, **10**, 72–76.

Paltridge, G. W., and C. M. R. Platt, 1976: Radiative processes in meteorology and climatology. *Developments in Atmospheric Science*, No. 5, Elsevier, 318 pp.

Steven, M. D., 1977: Standard distribution of clear sky radiance. *Quart. J. Roy. Meteor. Soc.*, **103**, 457–465.

Steyn, D., 1980: The calculation of view factors from fisheye-lens photographs. *Atmos.-Ocean*, **18**, 254–258.

Unsworth, M. H., and J. L. Monteith, 1975: Longwave radiation at the ground. *Quart. J. Roy. Meteor. Soc.*, **101**, 13–24.